Effective channel and ungauged braided river discharge estimation by assimilation of multi-satellite water heights of different spatial sparsity

P.-A. Garambois, Kévin Larnier, Jerome Monnier, Pascal Finaud-Guyot, Jonas Verley, Amanda Samine Montazem, Stephane Calmant

Effective channel and ungauged braided river discharge estimation by assimilation of multi-satellite water heights of different spatial sparsity

P.-A. Garambois(1)(2)*, K. Larnier(1)(4)(3)(5), J. Monnier (4)(5), P. Finaud-Guyot(1)(6), J. Verley(4)(5), A.-S. Montazem(1)(7)(8), S. Calmant (7)(8)

(1) Laboratoire des Sciences de l'ingénieur, de l'informatique et de l'imagerie (ICUBE), Fluid Mechanics Team, CNRS, Université de Strasbourg, France.

(2) INSA Strasbourg, Strasbourg, France.

(3) CS corporation, Business Unit Espace, Toulouse, France.

(4) Institut de Mathématiques de Toulouse (IMT), France.

(5) INSA Toulouse, France.

(6) ENGEES, Strasbourg, France.

(7) Laboratoire D'Etudes En Géophysique et Océanographie Spatiales (LEGOS, UMR 5566 CNES CNRS IRD UPS)

(8) Université de Toulouse III Paul Sabatier, OMP, Toulouse, France

Abstract

Multi-satellite sensing of continental water surfaces (WS) represents an unprecedented and increasing potential for studying ungauged hydrological and hydraulic processes from their signatures, especially on complex flow zones such as multichannel rivers. However the estimation of discharge from WS observations only is a very challenging inverse problem due to unknown bathymetry and friction in ungauged rivers, measurements nature, quality and spatio-temporal resolutions regarding the flow (model) scales. This paper proposes an effective 1D hydraulic modeling approach of sufficient complexity to describe braided river flows from sparse multisatellite observations using the HiVDI inverse method presented in Larnier et al. [42] with an augmented control vector including a spatially distributed friction law depending on flow depth. It is shown on $71km$ of the Xingu River (braided, Amazon basin) with altimetric water height timeseries that a fairly accurate upstream discharge hydrograph and effective patterns of channel bathymetry and friction can be infered simultaneously. The coherence between the sparse observation grid and the fine hydraulic model grid is ensured in the optimization process by imposing a piecewise linear bathymetry profile $b(x)$, which is consistent with the *hydraulic visibility* of WS signatures (Garambois et al. [27], Montazem et al. [46]). The discharge hydrograph and effective bathymetry-friction patterns are retrieved from 8 years of satellite altimetry (ENVISAT) at 6 virtual stations (VS) along flow. Next, the potential of the forthcoming SWOT data, dense in space, is highlighted by infering a discharge hydrograph and dense patterns of effective river bathymetry and friction; a physically consistent definition of friction by reaches enabling to consider more dense bathymetry controls. Finally a numerical analysis of the friction term shows clear signatures of river bottom slope break in low flows and width variations in high flows which is consistent with the findings of Montazem et al. [46] from WS curvature analysis

Keywords: Multichannel River, Ungauged River, 1D Hydraulic Model, Data Assimilation, Satellite Altimetry, SWOT, Hydraulic Visibility

* Corresponding author: pierre-andre.garambois@insa-strasbourg.fr

1. Introduction

Fresh water is a crucial earth's resource and its journey from the clouds to the oceans passes through the hydrographic network. In order to characterize hydrological fluxes, an essential physical variable is river discharge (cf. Global Climate Observing system et al. [22]) representing an integration of upstream hydrological processes. In complement of in situ sensors networks which are declining in some regions (e.g. Fekete and Vorosmarty [23]), increasingly accurate measurements of hydrological and hydraulic variables, and especially river surface variabilities are now enabled by myriads of satellites for earth observations and new generation of sensors (e.g. Vorosmarty et al. [56], Alsdorf and Lettenmaier [2], Calmant et al. [13], Schumann and Domeneghetti [54]).

The forthcoming Surface Water and Ocean Topography (SWOT) wide swath altimetric mission (CNES-NASA, planned to be launched in 2021) will provide a quasi global river surfaces mapping with an unprecedented spatial and temporal resolution on Water Surface (WS) height, width and slope - decimetric accuracy on WS height averaged over 1 km^2, 1 to 4 revisits every 21 days cycle 50, 5. In addition to decades of nadir altimetry (e.g. Frappart et al. [25], Birkett [6], Da Silva et al. [17], Calmant et al. [12]) and imagery (e.g. Allen and Pavelsky [1]) on inland waters, SWOT will enable an unprecedented *hydraulic visibility,* as defined from hydraulic analysis in Garambois et al. [27], Montazem et al. [47], Montazem et al. [46], of hydrological responses and hydraulic variabilities within river networks. Multi-satellite observations of water surfaces from the local to the hydrographic network scale indeed represent an unprecedented observability of hydrological responses through hydraulic processes signatures, especially on complex flow zones such as floodplains or braided rivers. This increased *hydraulic visibility* represents a great potential to learn hydrodynamic behaviors and infer hydrological fluxes.

The estimation of river discharge from water surface observations (elevations, top width) remains an open and difficult question, especially in case of unknown or poorly known river bathymetry, friction or lateral fluxes. Several open-channel inverse problems are studied in a relatively recent litterature in a satellite data context with more or less complex flow models and inverse methods (cf. Biancamaria et al. [5] for a review). Few studies started to highlight the benefit of assimilating synthetic SWOT WS observations in simplified hydraulic models with sequential methods, for infering inflow discharge assuming known river friction and bathymetry (Andreadis et al. [3], Biancamaria et al. [4]) or infering bathymetry assuming known friction (Durand et al. [19], Yoon et al. [58]). Next, low-complexity methods have been proposed for estimating river discharge in case of unknown bathymetry and friction based on the Manning-Strickler's law (Durand et al. [21], Garambois and Monnier [28]) or hydraulic geometries (Gleason and Smith [32]) or empirical flow models (Durand et al. [20], see also Bjerklie et al. [7]). They

are tested on 19 rivers with synthetic "SWOT-like" daily observations in 20 and their robustness and accuracy is found to fluctuate, the importance of good priors is highlighted; none of the tested river is braided.

The combined use of dynamic flow models and optimization methods enables to benefit from WS observations for solving hydraulic inverse problems as shown for flood hydrograph inference in Roux and Dartus [51] from WS width time series used to optimize a 1D hydraulic model or in Honnorat et al. [38], Hostache et al. [39], Lai and Monnier [41] by variational assimilation of flow depth time series in a 2D hydraulic model. The variational data assimilation (VDA) approach (see e.g. Cacuci et al. [11] and references therein) is well suited to solve the present inverse problem (see Brisset et al. [10], Oubanas et al. [48], Larnier et al. [42] and references therein).

It consists in fitting the hydraulic model response to the observed WS elevations by optimizing the "input parameters" in a variational framework. However, altimetry measurements of WS are relatively sparse in time compared to local flow dynamics. This important aspect of the inverse problem is investigated in Brisset et al. [10] with the introduction of *identifiability maps*. The latter consist to represent in space-time the available information: WS observables, hydraulic waves and an estimation of the misfit with local equilibrium. These "maps" enable to estimate if the sought upstream discharge information has been observed or not within the downstream river surface deformations; also they help to estimate inferable hydrograph frequencies Brisset et al. [10] or inferable hydrograph time windows Larnier et al. [42].

The inference of the hydraulic triplet (inflow discharge $Q(t)$, effective bathymetry $b(x)$ and friction coefficient K) from SWOT like WS observations is investigated in recent studies using 1D hydraulic and variational assimilation methods (e.g. Brisset et al. [10], Gejadze and Malaterre [29], Oubanas et al. [48], Larnier et al. [42]). However the inference of the triplet from WS observations remains a very challenging inverse problem because of the correlated influence of temporal (discharge) and spatial (bathymetry-friction) controls on the simulated flow lines. This is especially true because of the bathymetry-friction "equifinality issue", see the discussions in Garambois and Monnier [28], Larnier et al. [42]. Those recently developed VDA methods enable to infer accurately the inflow discharge from water surface observables, considering unknown/uncertain channel bathymetry-friction, but from accurate prior information and synthetic WS observations. Note that a strong prior such as a known stage-discharge relationship (rating curve) downstream of a river domain as it is done in [48] highly controls the simulated flow lines (fluvial regime); as a consequence the VDA process converge to the discharge hydrograph corresponding to the imposed (almost exact) rating curve. In the present study the downstream boundary condition is an unknown of the inverse problem.

A crucial point is the sensitivity of the triplet inference to the prior value from which the inference is started and it is only studied in a SWOT data context in Garambois and Monnier [28], Yoon et al. [59], Larnier et al. [42], Tuozzolo et al. [55]. The sensitivity of the estimated discharge (in the triplet) to the prior is highlighted by recent estimates performed from AirSWOT airborne measurements on the Willamette River (Tuozzolo et al. [55]). The temporal signal is well retrieved at observation times but using a biased prior hydrograph results in

a biased hydrograph inference - see detailed investigations in Larnier et al. [42]. In view to infer worldwide river discharge from the future SWOT observations, especially for ungauged cases, a hierarchical modeling strategy HiVDI (Hierarchical Variational Discharge Inversion) is proposed in Larnier et al. [42]. HiVDI approach includes low complexity flow relations (under the assumption of Low Froude and locally steady-state) which improve the robustness of the inferences in particular if an average value of Q is provided. (It may be provided by a database or a large scale hydrological model). Note that if introducing an a-priori information such as a single depth measurement, it enables to reconstruct an effective low-flow bathymetry see 30, 28, 42.

All the studies mentioned above address single thread natural rivers ($\sim$ 100km in length) without lateral inflows and using synthetic datasets (except in Tuozzolo et al. [55] with AirSWOT data). Moreover very few studies address the modeling of effective 1D channels from real satellite data (e.g. Garambois et al. [27], Schneider et al. [52]).

The present paper investigates the effective hydraulic modeling of braided river flows from real multi-sensor satellite observations of WS, the challenging inference of the hydraulic triplet ($Q(t)$, $b(x)$, $K(x,h)$) and its sensitivity to observation density in space. Multichannel rivers are characterized by complex hydraulic geometries relationships across flow regimes as shown in Schubert et al. [53] through an analysis of a metric resolution 2D shallow water model of a braided portion of the Platte River, US. The key point is to build up a sufficiently complex model to describe multichannel river flows and in coherence with satellite altimetry measurements spatio-temporal scales. Based on the inverse method presented in Larnier et al. [42], Brisset et al. [10], an effective hydraulic modeling strategy is adapted for tackling multichannel river flows using: (i) effective 1D cross sections based on real multi-satellite data from low to high flows (ii) a spatially distributed friction law depending on modeled water depth h. The inference of distributed hydraulic parameters patterns is investigated on a $71km$ long reach of the Xingu River (Amazone basin) from real altimetric observations along a single ENVISAT track or from synthetic SWOT observations, low *identifiability index* (as introduced in 10 and detailed in section 4). The influence of the spatial density of WS observations on the identifiability of spatial controls patterns (in the triplet) is studied. A piecewise linear bathymetry representation is introduced along with a friction power law with piecewise constant parameters to put in coherence the observations and the flow model grids. Their constraining effect on the inversions is studied with spatially sparse observations. Furthermore, numerical investigations are performed to test the sensitivity of hydraulic inferences to prior hydraulic values and also assess the correlated influence of bathymetry and friction on the modeled flow lines (equifinality) across flow regimes.

This study is organized as follows. Section 2 presents the 1D Saint-Venant flow model and the effective modeling approach for multichannel rivers including: (i) a spatially distributed friction law depending on modeled flow depth, (ii) the construction of an effective channel geometry from multi-satellite observations, (iii) an inverse method based on variational data assimilation. Section 3 focuses on the calibration of the effective model on 8 years of WS observations gained from ENVISAT altimeter on a single track along this braided river. Using this model as a reference, section 4 proposes detailed investigations of hydraulic inferences from real ENVISAT or synthetic SWOT

observations considering this braided river as ungauged. Section 5 presents numerical sensitivity analysis to the hydraulic prior and investigations on the bathymetry friction equifinality.

2. Effective hydraulic modeling approach:

This section proposes an original 1D modeling approach of adequate complexity for modeling multichannel river flows across regimes and in coherence with satellite observations. The approach is built on an effective channel cross section derived from multi-satellite measurements and a spatially distributed friction law depending on the flow depth.

2.1. The flow model

River flow is classically modeled using the 1D Saint-Venant shallow water equations involving an integration of the flow variables over the cross section (see e.g. Chow [15], Guinot [33] for detailed assumptions). In their non-conservative form in (A, Q) variables, A the wetted-cross section $\left[\mathrm{m}^2\right]$, Q the discharge $\left[\mathrm{m}^3.\mathrm{s}^{-1}\right]$, the equations read as follows [15]:

$$\begin{cases} \partial_t(A) + \partial_x(Q) & = 0 \\ \partial_t Q + \partial_x\left(\frac{Q^2}{A}\right) & = -gA\,\partial_x Z - gAS_f \end{cases} \tag{1}$$

where g is the gravity magnitude $\left[\mathrm{m.s}^{-2}\right]$, Z is the WS elevation [m], $Z = (b+h)$ with b is the river bottom elevation [m] and h is the water depth [m]. The friction term S_f is parameterized with the classical Manning-Strickler law such that $S_f = {}^{|Q|Q}/_{K^2A^2R_h^{4/3}}$ with K the Strickler friction coefficient $\left[\mathrm{m}^{1/3}.\mathrm{s}^{-1}\right]$, $R_h = {}^{A}/_{P_h}$ the hydraulic radius [m] , P_h the wetted perimeter. The discharge Q is related to the average cross-sectional velocity u $\left[\mathrm{m.s}^{-1}\right]$ such as $Q = uA$. A spatially distributed Strickler friction coefficient is defined as a power law in the water depth h:

$$K(x, h(x,t)) = \alpha(x) h(x,t)^{\beta(x)} \tag{2}$$

where α and β are two constants. Similar approaches based on hydraulic geometry or power law resistance equations are developed in the literature for predicting mean flow velocity for example on a wide range of in situ river flow measurements in Bjerklie et al. [8] or else for gravel bed streams in Ferguson [24]. The friction depends on the flow depth through the proposed power law relation (2) enabling a variation of friction effect in function of flow regime for complex flow zones for instance; this spatially distributed friction law is richer than a constant uniform value as it is often set in the literature from a-priori table of frictions in function of river types for instance (e.g. [14]).

The discharge $Q_{in}(t)$ is classically imposed upstream of the river channel. At downstream the Manning-Strickler equation depending on the unknowns $(A, Q; K)_{out}$ is imposed (it is classically integrated in the Preissmann scheme equations). The initial condition is set as the steady state backwater curve profile $Z_0(x) = Z(Q_{in}(t_0))$. This 1D

Saint-Venant model (1) is discretized using the classical implicit Preissmann scheme (see e.g. 16) on a regular grid of spacing Δx. It is implemented into the computational software DassFlow DassFlow.

2.2. Effective braided river model from long altimetric time series, satellite images and a hydrological model

A $L = 71km$ long portion of the Rio Xingu containing braided reaches is considered (figure 1, cf. Garambois et al. [27],). WS observations are available at 6 virtual stations along a single ENVISAT track (#263) representing 77 samples of WS profiles between mid 2002 and mid 2010 (cf. Da Silva et al. [17]); that is $\left\{Z_{s,p}^{obs}\right\}_{S,P}^{env}$ with $S = 6$ corresponding to the locations of the virtual stations simultaneously observed at $P = 77$ times (see table 1).

An effective hydraulic modeling strategy of this braided river is proposed based on:

- Cross-sectional water surface widths $\{W\}_{S,2}^{jers}$ obtained from JERS mosaics (Courtesy of GRFM, NASDA/MITI) in low and high flows. The effective water surface width is the sum of the width of all individual river channels for braided reaches.

- An a priori river bottom $\{b\}_{r_{VS}}$ obtained from altimetric rating curves from Paris et al. [49]. They are determined by adjusting the parameters of a classical stage discharge relationship on WS elevations gained by satellite altimetry and discharge simulated with the large scale hydrological model MGB (de Paiva et al. [18]) on the temporal window of interest - called true discharge in what follows.

Effective cross-sections geometries are defined at the 6 virtual stations with the bathymetry b given by altimetric rating curves and from effective widths such that low flow width (resp. high flow) is reached for the first (res. ninth) decile of observed WS elevations for each cross section. The final model geometry is obtained by linear interpolation between these 6 effective cross sections on the model grid with $\Delta x = 50m$. It is shown in Fig. 1 along with ENVISAT and SWOT spatial samplings. The friction law 2 introduced above and depending on the flow depth h is distributed using patches with constant values for each reach between two successive virtual stations.

2.3. The computational inverse method

This paper investigates the estimation of the hydraulic triplet ($Q(t)$, $b(x)$, $K(x,h)$) from observations of WS variabilities only on a braided river. The employed inverse method is those presented in Larnier et al. [42] (see also Brisset et al. [10]) with an augmented composite control vector c; it is detailed in Appendix 7. c contains a spatially distributed friction coefficient enabling to model complex flow zones (while it is an uniform friction law $K(h)$ in Larnier et al. [42]). This definition of $K(x,h)$ enables to consider more heterogeneous bathymetry controls.

The principle is to estimate (discrete) flow controls minimizing the discrepancy between Z_{obs} the observed flow line and Z the modeled one; the latter depending on the unknown parameters vector c through the hydrodynamic model (1). This discrepancy is quantified through the cost function term $j_{obs}(c) = \frac{1}{2}\|Z_{obs} - Z(c)\|_2^2$, see Appendix

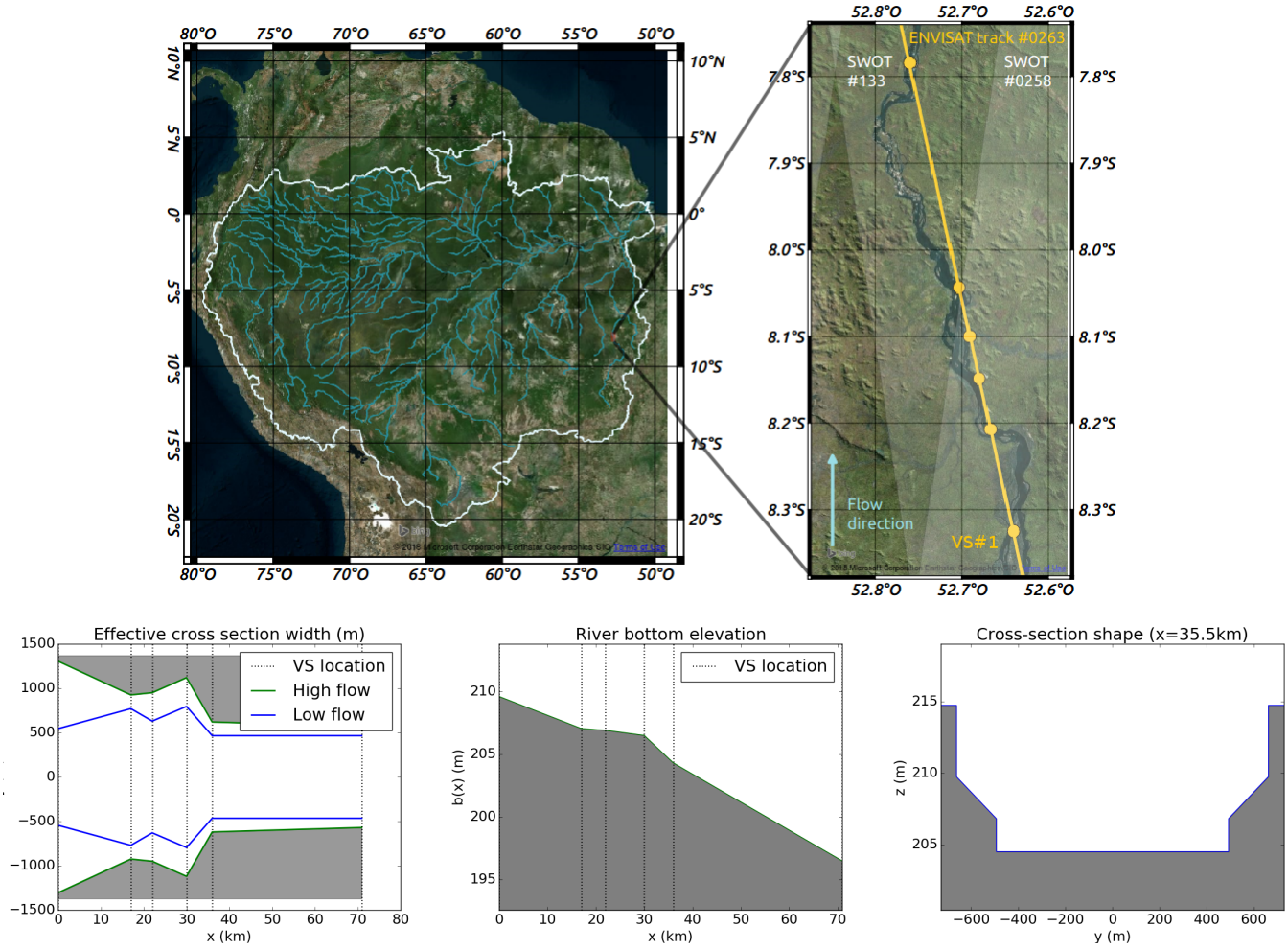

Figure 1: Study zone (top) with ENVISAT track #263 and virtual stations (orange dots); simulated SWOT tracks #133 and #258 on the 1^{st} and 6^{th} day every 21 days repeat cycle (transparent white). Effective river bathymetry derived from altimetric rating curves (Paris et al. [49]) and water surface width from satellite images.

7 for details. The control vector c contains the unknown "input parameters" of the 1D Saint-Venant shallow water flow model (eq. 1) considering effective cross sections (see figure 1). In the present study, c reads as:

$$c = (Q_{in,0},\ ...,\ Q_{in,P};\ b_1,\ ...,\ b_R;\ \alpha_1,\ ...,\alpha_N,\ \beta_1,\ ...,\beta_N)^T \tag{3}$$

where temporally and spatially distributed controls are the upstream discharge $Q_{in,p}$, the river bed elevation b_r and the distributed friction parameters α_n and β_n.

The subscript p denotes the observation time $p \in [0..P]$ and r denotes the reach number, $r \in [1..R]$.

α_n and β_n are the parameters of the friction law depending on the model state h (2) for each patch $n \in [1..N]$ with $N \leq R$.

The inversion consists to solve the following minimization problem: $c^* = \text{argmin j}(c)$ (eq. 8).

This minimization, optimization problem is solved using a first order gradient-based algorithm, more precisely the classical L-BFGS quasi-Newton algorithm.

3. Calibration of the effective hydraulic model on historical satellite altimetry

Thi section presents the calibration of the effective hydraulic model based on the reference effective geometry defined above (cf. section 2.2). The observed water elevation time series $\{Z_{s,p}^{obs}\}_{S,P}^{env}$ at $S = 5$ ENVISAT virtual stations are used to calibrate the friction law of the 1D Saint-Venant flow model (1). Since friction has a local and upstream influence on the flow line (low Froude fluvial flows, figure 9) the remaining ENVISAT time series at VS#6 downstream of the river domain will be used for infering the full control vector c in next section - recall that a normal depth is used as downstream BC (cf. section 2.1).

A "reduced" control vector $c_{cal} = (\alpha_1,\ ...,\alpha_N,\ \beta_1,\ ...,\beta_N)$ consisting in spatially distributed friction parameters only is considered here. In order to avoid a spatial "overparameterization" regarding the 5 water height timeseries available at VS, the choice is made to spatialize friction on $N = 5$ patches, on each reach downstream an altimetric VS. The inverse method presented in Larnier et al. [42] and described in appendix (section 7) is used here with no regularization nor variable change for this "simple" calibration problem.

An optimal friction distribution c_{cal}^* is found with the inverse method and the calibrated values of $\alpha_{n=1...5}$ and $\beta_{n=1...5}$ are summed up in table 1. The resulting water height time series are compared to altimetric observations for each virtual station (cf. figure 2). The spatially distributed friction law 2 enables a fairly good reproduction of the observed water level variations on this braided river, across a wide range of flow regimes, even with an effective 1D model built on multi-satellite data (fig. 2).

A constant friction in time would lead to systematical errors for a large range of flows as shown by grey curves on figure 2. The calibrated friction exponents β_n range between 0.482 and 1.133 except for the second reach (SV2-3) where a small β_n is found, that is a barely constant friction across flow regimes for this small reach (cf. fig. 2). The

Virtual station name	VS#1	VS#2	VS#3	VS#4	VS#5	VS#6
Flow distance to mouth [km]	1146	1129	1124	1116	1110	1075
Flow distance from the upstream [km]	0	17	22	30	36	71
Drainage area [km^2] (MGB model)	193.255	193.255	194.148	194.148	195.882	197.862
Z_0 [m] (reference : EGM2008) (Paris et al. 2016)	209.6	207.1	206.9	206.5	204.3	196.5
$W_{low}(x)$ Total low flow width [m] (derived from JERS)	1090	1540	1260	1590	930	930
$W_{high}(x)$ Total high flow width [m] (derived from JERS)	2610	1850	1900	2240	1240	1140
Calibrated friction factor $\alpha^{cal}(x)$ (downstream reach)	12.785	19.574	9.869	4.252	7.425	-
Calibrated friction exponent $\beta^{cal}(x)$ (downstream reach)	0.482	0.071	0.624	1.133	0.718	-

Table 1: Summary of the effective hydraulic model parameters including calibrated friction parameters $\alpha^{cal}(x)$ and $\beta^{cal}(x)$ (recall $K(x,h) = \alpha(x)h^{\beta(x)}$) using 8 years of WS elevation variations (ENVISAT data) given effective channel bathymetry and upstream discharge from the MGB hydrological model (de Paiva et al. [18]).

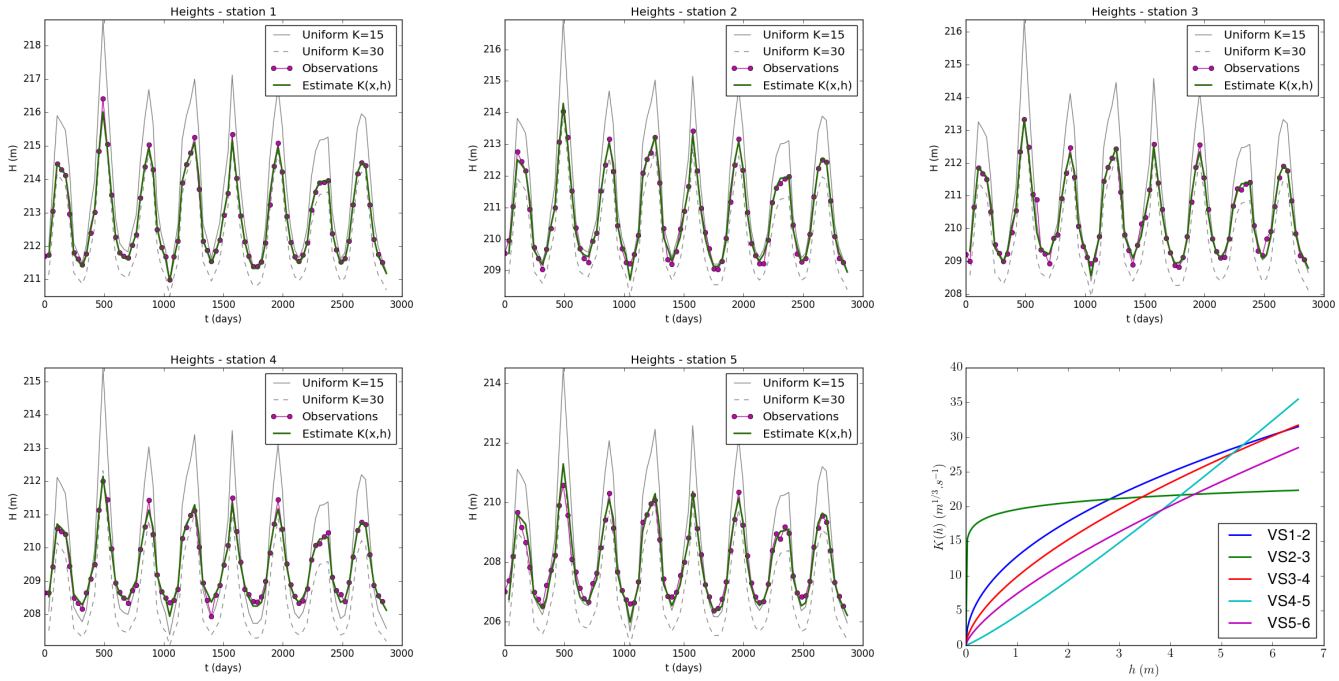

Figure 2: Calibration of variable friction $K(x,h)$ with 8 years of ENVISAT measurements at 6 VS using the variational method with $c = (\alpha_1, ..., \alpha_5, \beta_1, ..., \beta_5)$; $j_{obs} = 0.07$. (Bottom right) Effective friction law in function of water depth for each VS.

spatial pattern of α_n values calibrated here correspond to significant friction effects, varying across flow regimes, and necessary to effectively represent braided reaches using a 1D effective cross section. Indeed the latest leads to an underestimation of the hydraulic radius $R_h = {}^{A}/_{P_h}$ hence of the friction term $S_f = {}^{|Q|Q}/_{K^2A^2R_h^{4/3}}$ in the 1D Saint-Venant model (see section 2.1) for braided reaches.

4. Investigations on the inference from WS observations of distributed flow controls on braided river flows

This section studies the challenging inference of the hydraulic triplet (discharge, bathymetry, friction) from multi-satellite WS observations. The braided Xingu River morphology represents a supplementary difficulty for inversions regarding the variability of local hydraulic behaviors accross flow regimes as evidenced above by the calibrated

friction laws ($\beta^{cal} \neq 0$). The impact of spatial controls density and bathymetry representation is asssessed in what follows regarding the spatial sparsity of observations. First is presented the numerical experiment framework, then the inferences with relatively "sparse" ENVISAT measurements and finally those with SWOT synthetic observations.

4.1. Inverse hydraulic modeling method with WS elevations gained from nadir altimetry and SWOT

The effective hydraulic model described in section 2.2 and calibrated in section 3 is used as a reference ("*target*") in the following numerical experiments. The control vector (eq. 3) containing discharge, bathymetry and friction is sought with the inverse method decsribed in section 2.3 (see also appendix, section 7). It is tested first with real ENVISAT time series repesenting a relatively sparse spatial sampling of WS signatures with 6 VS on this $71km$ long river, and next with synthetic SWOT observations sampling the flow line at $\Delta x = 200m$ (RiverObs product, see Frasson et al. [26]).

The Xingu River is observed either by a single along-stream ENVISAT track at 6 observation points (virtual stations) of flow lines every 35 days, or two SWOT tracks providing dense WS observations in space twice per 21 days repeat cycle (5 days delay, cf. section 2.2). Note that the temporal sparsity of observations (35 days for ENVISAT or 5 days between the two SWOT passes every 21 days) only enables to identify low hydrograph frequencies, at observation times (see Brisset et al. [10] for a detailled analysis and identifiability maps). Indeed the hydraulic wave propagation time is around $T_{wave} \sim 9h$ which is much smaller than the lowest satellite revisit time of 5 days. This propagation time is calculated using the kinematic wave velocity for rectangular channels $c_k = 5/3U$ and maximal high flow velocity $U = 2,17\text{m/s}$ from calibrated model outputs $c_k = 2.2\text{m/s}$ (second hydrograph peak at $t = 490\,days$, see flow variables on figure 9). Let $I_{indent} = T_{wave}/\Delta t_{obs}$ be the identifiability index defined in Brisset et al. [10] as the ratio between flood wave propagation time and observation time step. This leads to a very low temporal identifiability index for this $71km$ river: $I_{ident} = 7.5 \times 10^{-2}$ for SWOT and $I_{ident} = 10^{-2}$ for ENVISAT. Consequently, only low temporal dynamics and discharge at observation times are inferable as shown in Brisset et al. [10]; SWOT and ENVISAT observations are thus considered separately in the present study.

The starting point of the VDA process in the parameter space, the so-called prior c_{prior} (cf. section 7), consists in a rough hydrological prior: $Q^{(0)} = \overline{Q}_{MGB}$ the mean discharge estimated from the MGB hydrological model, a spatially constant $\alpha^{(0)}$ friction defined a priori from classical hydraulic ranges (e.g. Chow [14]) and $\beta^{(0)} = 1$, the bathymetry $b^{(0)}$ is defined as a simple straight line over the whole domain for hydraulic analysis first. Note that the sensitivity of the inference to the prior definition is investigated in section 5.

In a noised observation context, we denote by δ the noise level such that $\|Z_{obs} - Z_{true}\|^2 \leq \delta$ for all spatial locations r with Z_r^{obs} the observed and Z_r^{true} the true WS elevation. A common technique to avoid overfitting noisy data, in the context of Tykhonov's regularization of ill-posed problems, is Morozov's discrepancy principle, (see e.g. Kaltenbacher et al. 40 and references therein): the regularization parameter γ (see eq. 6) is chosen *a-posteriori* such that j does not decrease below the noise level. In the present numerical experiments, the convergence is stopped if $j_{obs}(c) \leq 10^{-1}$ or if j_{obs} is not decreased anymore for higher discrepencies.

4.2. Inference of distributed hydraulic controls $(Q(t), K(x,h), b(x))$ with spatially sparse WS observations: real ENVISAT altimetric snapshots

In this section the assimilation is based on WS elevations $\left\{Z_{s,p}^{env}\right\}_{S,P}$ at $S = 6$ virtual stations observed simultaneously by ENVISAT during 8 years every 35 days, i.e. $P = 77$. In this spatially sparse observation context, the impact of spatial controls density is investigated.

First, we consider a "full" control vector c (cf. eq. 3) including $P = 77$ inflow discharges, all 1D model bathymetry points $R = 1420$ and $N = 5$ friction patches between ENVISAT virtual stations (cf. section 2.2). The infered inflow discharge, bathymetry and friction are presented in figure (3) (case Env.a). Despite the satisfying value of the hydraulic controls reached at iteration 35, the descent is still possible as shown by j_{obs} decreasing of about 20% at iteration 96. Allthough it enables to fit the observations according to the a priori convergence criteria defined in section 4.1, the solution found after the VDA process is not very accurate nor realistic as shown by peak flow underestimations and significant oscillations of the identified friction and bathymetry. The spatial sparsity of observations prevents to infer these relatively dense bathymetry controls; in this case the considered inverse problem is underconstrained.

In order to better constrain the inverse problem in case of sparse spatial observability, a bathymetry representation is consistently introduced at the scale of the observation grid and applied to the finer flow modeling grid. Based on the physical analysis of the SW model (1) behaviour and the WS signature of bathymetry/friction controls (see Montazem et al. [47], Montazem et al. [46], Montazem [45]), a linear bathymetry interpolation is used between successive couples of bathymetry controls defined at observation points only. The resulting bathymetry $\tilde{b}(x) \in \mathcal{C}^0(\mathbb{R}), \forall x \in [0, L]$ is piecewise linear and strongly constrains the bathymetry profile between the sought bathymetry points - instead of using only a weak constrains $j_{reg}(c) = \frac{1}{2} \left\| b"(x) \right\|_2^2$ in the optimization process (cf. appendix 7) as done in the next section 4.3 with spatially dense SWOT observations. Using this bathymetry constrain with $R = 6$ bathymetry controls defined at each ENVISAT virtual station results in 5 reaches and $N = 5$ friction patches are consistently applied to each. This leads to a more robust and accurate inference as shown in Figure 4 (case Env.b). The discharge infered for 8 years is fairly correct (RMSE $= 520\,\mathrm{m}^3/\mathrm{s}$, Nash $= 0.95$) and relatively realistic bathymetry/friction patterns are found, with some compensations between spatial controls locally in space, which is further analyzed in what follows.

The impact on the infered parameters of searching a spatially uniform friction law is tested with the piecewise linear bathymetry representation used above. The resulting discharge inference is fairly correct (RMSE $= 608\,\mathrm{m}^3/\mathrm{s}$, Nash $= 0.93$) and interestingly the bathymetry spatial pattern is well retrieved but shifted above the reference one (cf. figure 5) (case Env.c). The infered friction coefficients are $\alpha = 22.621$, $\beta = 0.217$, which represents a lower friction effect on most flow regimes regarding the calibrated ones (cf. table 1). This infered effective friction law and bathymetry pattern, leading to somehow effective stage-discharge relationships locally given the infered hydrograph, enable to approximate the observed WS variations ($j_{obs} = 1.269$) but with a less accurate fit than with spatially

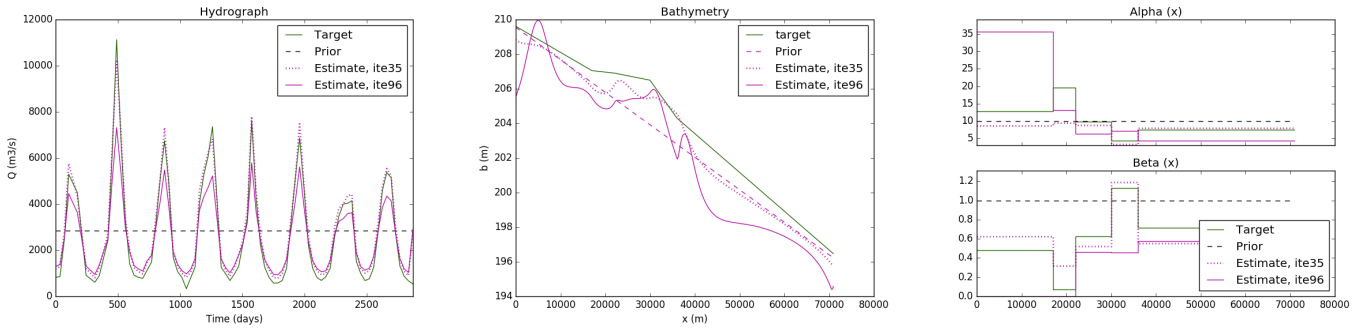

Figure 3: Identification of $(Q(t), K(x,h), b(x))$ with ENVISAT observations and overparameterized $c = \left(Q_{in,0}, ..., Q_{in,P}; b_1, ..., b_R; \alpha_1, ..., \alpha_N, \beta_1, ..., \beta_N\right)^T$ with $P = 77$, $R = 1420$, $N = 5$, bathymetry regularization weight $\gamma = 10^{-3}$; $j_{obs} = 0.098$ at iteration 35 (top) and $j_{obs} = 0.077$ at iteration 96 (bottom) (Env.a)

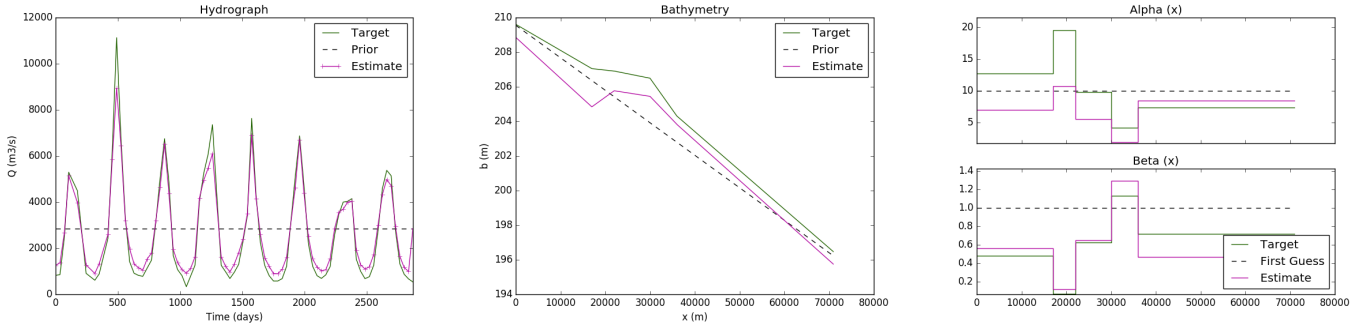

Figure 4: Identification of $(Q(t), K(x,h), b(x))$ with ENVISAT observations and effective $c = \left(Q_{in,0}, ..., Q_{in,P}; b_1, ..., b_R; \alpha_1, ..., \alpha_N, \beta_1, ..., \beta_N\right)^T$ with $P = 77$, $R = 6$, $N = 5$ with a piecewise linear bathymetry $b(x)$ reconstruction, $\gamma = 0$; $j_{obs} = 0.118$ at iteration 51. (Env.b)

distributed friction ($j_{obs} = 0.118$). Note in that case of a lower model complexity an underestimation of the low flow discharges.

These infered friction laws and bathymetry patterns - simultaneously infered with the discharge hydrograph - correspond to "effective rivers" enabling to fit the observed variability of flow lines. Recall that the observations consist in real measurements of WS elevations gained by nadir altimetry on multichannel reaches of the Xingu River. The complexity of the forward-inverse modeling approach, in coherence with the spatial sparsity of observation grid, enables to approximate satisfactorily the one of the observed multichannel flow. The additionnal constrain provided by spatially dense flow lines observations is investigated in the next section with SWOT synthetic data.

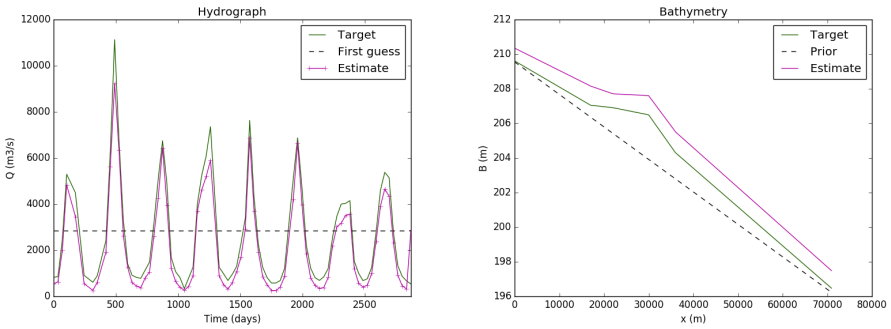

Figure 5: Inferrence of $Q(t)$, $b(x)$ and spatially uniform $K(h) = \alpha h^{\beta}$ with ENVISAT WS observations and effective $c = \left(Q_{in,0}, ..., Q_{in,P}; b_1, ..., b_R; \alpha, \beta\right)^T$, $P = 77$, $R = 6$, no bathy $\gamma = 0$; $j_{obs} = 1.269$ at iteration 54. The identified friction coefficients are $\alpha = 22.621$, $\beta = 0.217$. (Env.c)

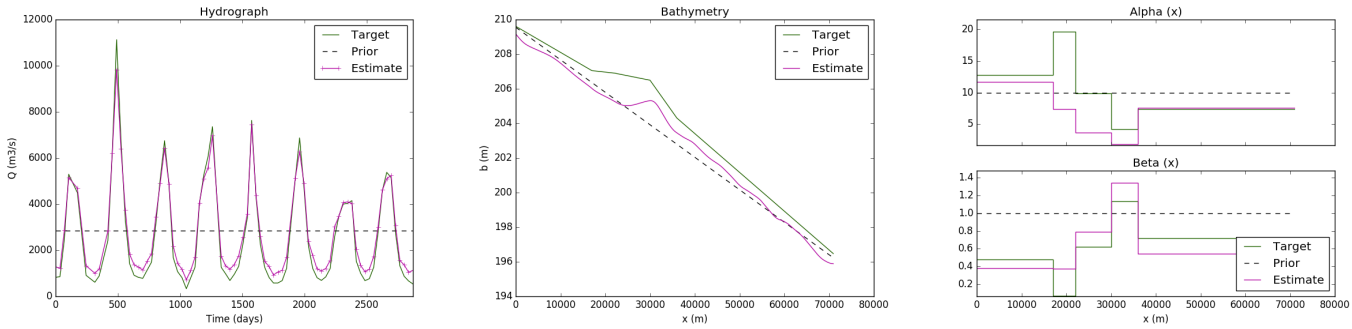

Figure 6: Identification of $(Q(t), K(x, h(x,t)), b(x))$ with SWOT-sge observations and effective $c = (Q_{in,0}, ..., Q_{in,P}; b_1, ..., b_R; \alpha_1, ..., \alpha_N, \beta_1, ..., \beta_N)^T$ with $P = 276$, $R = 1420$, $N = 1419$, $\gamma = 10^{-3}$; $j_{obs} = 0.099$ at iteration 41. (SWOT.a)

4.3. Inference of distributed hydraulic controls $(Q(t), K(x,h), b(x))$ with spatially dense WS observations: SWOT synthetic observations

In this section the full hydraulic control c (cf. eq. 3) is infered by assimilating SWOT-like observations. Those noisy data are computed using the SWOT hydrology simulator applied to flow lines from the effective hydraulic model calibrated above (cf. section 3). The SWOT spatio-temporal pattern over the studied river is obtained by overlapping the river centerline and the expected SWOT orbit and swaths (cf. figure 1). Finally the synthetic SWOT-like observables consist in WS elevations $\left\{Z_{obs}^{SWOT}\right\}_{r,p}$ with $p \in [1..P]$ and $P = 276$ generated on the fine scale model grid i.e. $r \in [1..1420]$.

The inflow discharge, bathymetry and friction are infered by assimilating SWOT WS observations $\left\{Z_{obs}^{SWOT}\right\}_{r,p}$ on the same spatial grid as that of the numerical hydraulic model with c_{prior1}. The estimates are presented on figure (6). The infered discharge hydrograph is accurate (RMSE $= 391\,\mathrm{m}^3/\mathrm{s}$, Nash $= 0.97$) and bathymetry/friction patterns are relatively well retrieved. Using SWOT spatially distributed observations and piecewise constant roughness enable to constrain the inference of bathymetry controls at a fine spatial resolution (model grid); the inverse method including covariance matrices acting as spatial or temporal smoothers/regularizations (cf. eq. 11 in appendix). The infered discharge and the spatially distributed controls are slightly more accurate than previously in a comparable inversion scenario with sparse ENVISAT observations in space and piecewise linear bathymetry constrain (case Env.b, cf. table 2 and figure 4). Note that the friction is sought by reaches which enables to consider more dense bathymetry controls. Again, the compensation between spatial controls appears locally in space but enables the best fit to distributed measurements of WS elevations given the infered discharge ($j_{obs} = 0.099$).

5. Numerical investigation of the bathymetry-friction equifinality

The hydrograph is responsible for flow variability in time, hence enabling to retrieve the temporal dynamics of the observed flow lines (Brisset et al. [10], Larnier et al. [42]). The friction and bathymetry controls have a correlated influence on the modeled flow lines therefore leading to an ill-posed inverse problem (cf. Garambois and Monnier [28], Larnier et al. [42] for investigations on this "*bathymetry-friction equifinality*" in a comparable data-inversion context). In this section the influence of the prior value on the quality of the inferences with spatially distributed controls is investigated. Next, is proposed a numerical analysis of the sensitivity of the friction source term S_f in the Saint-Venant equations (1) to the flow controls (triplet) that are embeded in it.

5.1. Sensitivity to the prior of the hydraulic inference from altimetric observations of WS signature

Given altimetric measurements of WS variabilities and the first guess c_{prior1}, the inverse method enables to infer a complex control vector composed of temporally and spatially distributed controls of the 1D SW model (1). In the numerical experiments above, the discharge hydrograph $Q(t)$ is accurately infered at observation times but because of the ill-posedness of the inverse problem, compensations can occur between the sought parameters and especially between the spatial controls - the bathymetry $b(x)$ and the distributed friction parameters $\alpha(x)$ and $\beta(x)$. As already pointed out in the VDA inferences performed with the DassFlow model using SWOT like data in (Brisset et al. [10], Larnier et al. [42]) and AirSWOT data (Tuozzolo et al. [55]), the accuracy of the inferred discharge depends on the quality of the prior.

The sensitivity of the inference to the quality of the prior control vector is investigated here for the most challenging inverse problem with spatially distributed controls and sparse ENVISAT data. First the inflow prior is varied of $\pm 30\%$ around the mean true discharge; the river bottom elevation and friction priors are set as previously in c_{prior1}. The infered hydraulic controls are presented in 7 and various inference scores are sumed up in table 2. For each inflow prior, the temporal variations of the inflow hydrograph are very well retrieved as shown on figure 7 - runs Env.b2 and Env.b3. However a biased inflow prior results in a biased hydrograph estimate (with correct temporal variations) which is coherent with results of Larnier et al. [42], Tuozzolo et al. [55]).

Next, the sensitivity to the prior bathymetry and friction is tested. The prior bathymetry is infered with the low-complexity system proposed in the hierarchichal HiVDI model chain (Larnier et al. [42]) for ungauged rivers. It consists in estimating an effective prior bathymetry from WS observables using the low Froude model and prior discharge from a hydrological model ($\overline{Q_{MGB}}$ here) and prior friction ($\alpha^{(0)}, \beta^{(0)}$). Two prior c_{man1} and c_{man2} are considered with prior friction under/over-estimations compared to calibrated ones (cf. 8). As shown on figure 8, the inference in case Env.b31 (blue) results in an accurate estimation of discharge, very similar to Env.b (purple). It is started from a prior c_{man1} that underestimates river bottom elevation and overestimates the spatially averaged friction effect compared to calibrated values (cf. figure 8, bottom). In that case, fitting WS elevations enables to infer an effective river channel (bathymetry and friction) but also to infer a fairly realistic upstream temporal

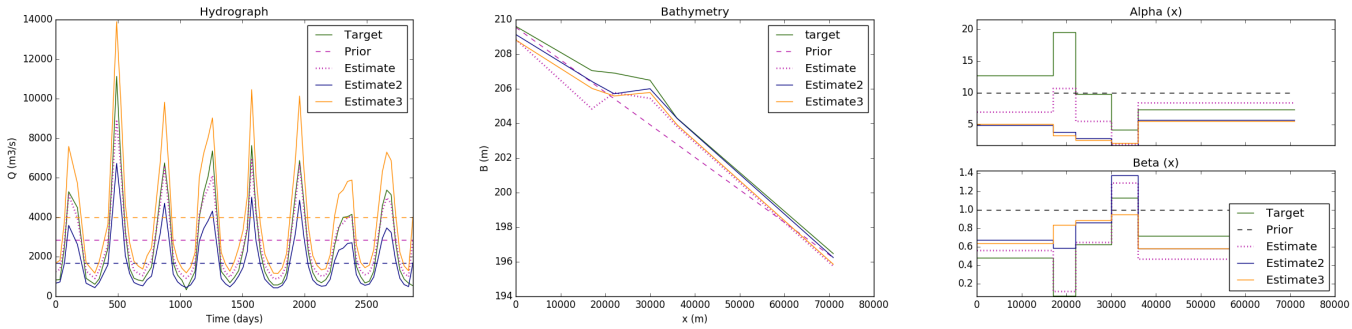

Figure 7: Sensitivity test to prior discharge $\overline{Q_{MGB}}\pm30\%$; identification (var change) of $(Q(t), K(x,h), b(x))$ with ENVISAT observations $c = \left(Q_{in,0},\ ...,\ Q_{in,P};\ b_1,\ ...,\ b_R;\ \alpha_1,\ ...,\alpha_S,\ \beta_1,\ ...,\beta_S\right)^T$ with $P = 77$, $R = 6$, $N = 5$ and with a piecewise linear b(x) and $S = R = 5$. "Estimate" (case Env.b) $j_{obs} = 0.118$ at iteration 51, "Estimate2" (case Env.b21) $j_{obs} = 0.125$ at iteration 41, "Estimate3" (case Env.b21) $j_{obs} = 0.125$ at iteration 25.

control (discharge hydrograph). Using the prior c_{man2} that overestimates both river bottom elevation and spatially averaged friction effect results in a comparable fit to the observed WS elevations. However this correct fit stems from the compensation between an infered effective channel of reduced conveyance capacity (comparable friction effects but overestimated bed levels) and consequently an infered hydrograph with underestimated low-flow discharges (in yellow).

5.2. Spatio-temporal sensitivity of the friction term

The considered flow controls $(Q(t),\ K(x,h),\ b(x))$ of the 1D Saint-Venant shallow water equations (1) have a complex non linear influence on the modeled flow line and consequetly on the fit to the observed flow lines. The variation of momentum expressed by the second flow equation is due to a pressure source term $-gA\,\partial_x Z$ (including the longitudinal variation of fluid-to-fluid pressure, the longitudinal variation of lateral and bottom wall-to-fluid pressure) and a dissipation term $-gAS_f$. Discharge and bathymetry appear in the momentum and pressure terms while all flow controls are embedded in the friction source term S_f. Note that for a locally steady uniform flow $S_f = -\partial_x Z$ and an infinity of friction and bathymetry values can correspond to a single value of discharge (cf. Garambois and Monnier [28], Larnier et al. [42]).

We propose a simple calculation in order to make appear the sensitivity of the friction term to a change on controls; let us express the differential of S_f assuming $Q > 0$:

$$\begin{aligned} \mathrm{d}S_f &= \mathrm{d}\left(\frac{1}{K^2}\frac{Q^2}{A^2R_h^{4/3}}\right) \\ &= -\frac{2}{K^3}\frac{Q^2}{A^2R_h^{4/3}}\mathrm{d}K - \frac{2}{A^3}\frac{Q^2}{K^2R_h^{4/3}}\mathrm{d}A - \frac{4}{3R_h^{7/3}}\frac{Q^2}{K^2A^2}\mathrm{d}R_h + \frac{1}{K^2}\frac{2Q}{A^2R_h^{4/3}}\mathrm{d}Q \end{aligned} \tag{4}$$

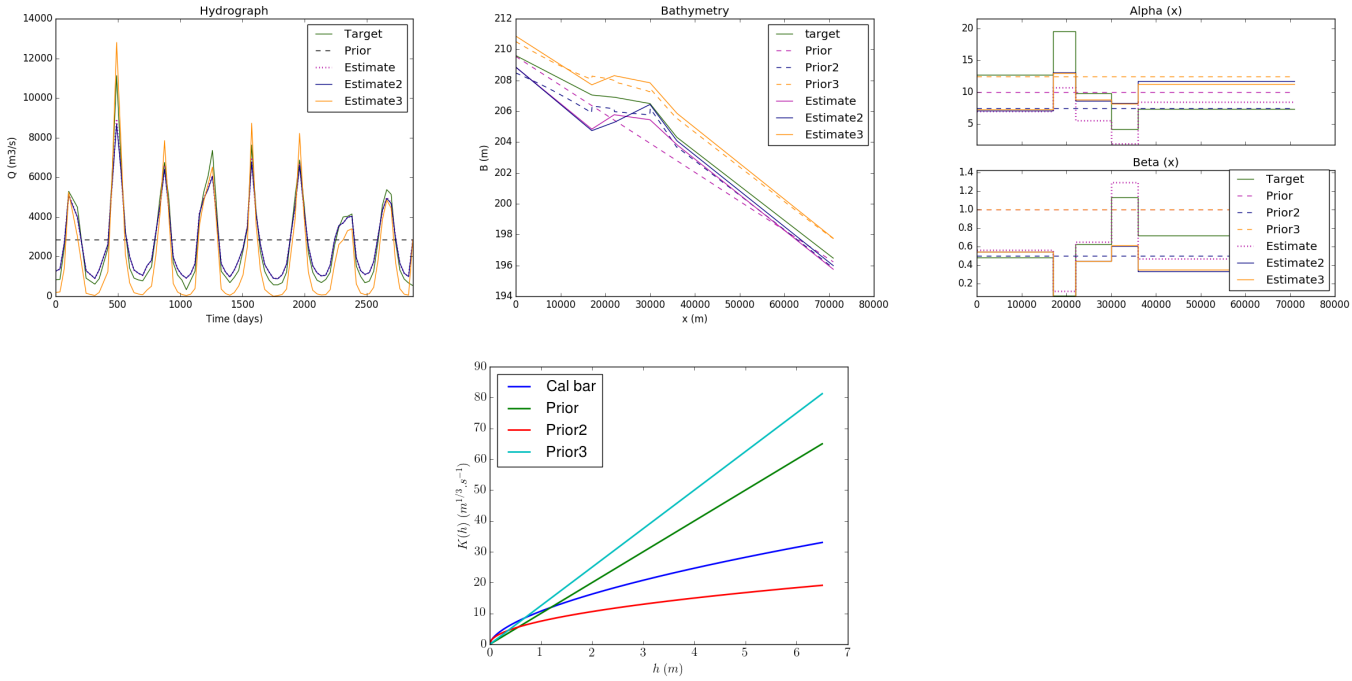

Figure 8: Sensitivity test to prior friction and bathymetry estimated using the "Manning" method from Larnier et al. [42] (c_{man1} ($\alpha^{(0)} = 7.5$; $\beta^{(0)} = 0.5$) and c_{man2} ($\alpha^{(0)} = 12.5$; $\beta^{(0)} = 1$)); identification (var change) of $(Q(t), K(x,h), b(x))$ with ENVISAT observations $c = \left(Q_{in,0}, ..., Q_{in,P}; b_1, ..., b_R; \alpha_1, ..., \alpha_S, \beta_1, ..., \beta_S\right)^T$ with $P = 77$, $R = 6$, $N = 5$ and with a piecewise linear b(x) and $S = R = 5$. "Estimate" (case Env.b) $j_{obs} = 0.118$ at iteration 51, "Estimate2" (case Env.b31) $j_{obs} = 0.116$ at iteration 46, "Estimate3" (case Env.b32) $j_{obs} = 0.122$ at iteration 41. (Bottom) prior effective friction laws and spatially averaged calibrated friciton law ($\overline{\alpha_{cal}} = 10.74$ and $\overline{\beta_{cal}} = 0.6$, "Cal bar").

Case	Control	Prior	$\text{RMSE}_{\text{Q}^{(0)}}$ (m^3/s)	$r\text{RMSE}_{\text{Q}^{(0)}}$ (%)	$\text{Nash}_{\text{Q}^{(0)}}$ $(-)$	$\text{RMSE}_{\text{b}^{(0)}}$ (m)	$\text{RMSE}_{\alpha^{(0)}}$ $(m^{1/3-\beta}/s)$	$\text{RMSE}_{\beta^{(0)}}$ $(-)$
Env.a	Dense $b(x)$	c_{prior1}	2254	194	-0.01	1.19	4.93	0.49
Env.b	Piec. $b(x)$	c_{prior1}	"	"	"	"	"	"
Env.c	Piec. $b(x)$, $K(h)$	c_{prior1}	"	"	"	"	"	"
SWOT.a	Dense $b(x)$	c_{prior1}	"	"	"	"	"	"
Env.b21	Piec. $b(x)$	$Q^{(0)}_{prior1} - 30\%$	2433	97	0.18	1.19	4.93	0.49
Env.b22	Piec. $b(x)$	$Q^{(0)}_{prior1} + 30\%$	2626	297	-0.37	"	"	"
Env.b31	Piec. $b(x)$	c_{man1} ($\alpha^{(0)} = 7.5$; $\beta^{(0)} = 0.5$)	2254	194	-0.01	0.77	5.63	0.34
Env.d32	Piec. $b(x)$	c_{man2} ($\alpha^{(0)} = 12.5$; $\beta^{(0)} = 1$)	2254	194	-0.01	1.13	5.43	0.49

Case	Control	Prior	RMSE_{Q} (m^3/s)	rRMSE_{Q} (%)	Nash_{Q} $(-)$	RMSE_{b} (m)	RMSE_{α} $(m^{1/3-\beta}/s)$	RMSE_{β} $(-)$
Env.a	Dense $b(x)$	c_{prior1}	830	57	0.86	1.97	10	0.46
Env.b	Piec. $b(x)$	c_{prior1}	520	61	0.95	1.07	4.8	0.37
Env.c	Piec. $b(x)$, $K(h)$	c_{prior1}	608	58	0.93	1.05	–	–
SWOT.a	Dense $b(x)$	c_{prior1}	391	38	0.97	0.91	5.67	0.2
Env.b2	Piec. $b(x)$	$Q^{(0)}_{prior1} - 30\%$	1229	39	0.7	0.48	7.83	0.28
Env.b3	Piec. $b(x)$	$Q^{(0)}_{prior1} + 30\%$	1473	104	0.57	0.75	5.09	0.22
Env.bm2	Piec. $b(x)$	c_{man1} ($\alpha^{(0)} = 7.5$; $\beta^{(0)} = 0.5$)	550	61	0.94	1.22	4.64	0.32
Env.bm3	Piec. $b(x)$	c_{man2} ($\alpha^{(0)} = 12.5$; $\beta^{(0)} = 1$)	885	78	0.84	1.30	5.50	0.35

Table 2: Scores of the inferences (bottom) performed with various priors (top), ENVISAT ("Env") or SWOT ("SWOT") observations.

Since $\mathrm{d}R_h = \mathrm{d}(A/P) = \frac{1}{P}\mathrm{d}A - \frac{A}{P^2}\mathrm{d}P = \frac{1}{P}\left(\mathrm{d}A - R_h\mathrm{d}P\right) = \frac{1}{P}\left(\mathrm{d}A_0 - R_h\mathrm{d}P_0\right) + \mathrm{d}f(h)$ with $A_0 = W_0 h_0$ and $P_0 = W_0 + 2h_0$ respectively the unobserved low flow area and perimeter under our modeling hypothesis (cf. section 2.2 and figure 1, see also Larnier et al. [42] for details on cross section representation). It follows that $f(h)$ is a function depending on the modeled water depth h and of the observed cross-section variation δA above low flow (h_0), W_0 being defined from observables. We get $\mathrm{d}R_h = \frac{1}{P}\left(1 - \frac{2R_h}{W_0}\right)\mathrm{d}A_0 + \mathrm{d}f(h)$ and finally:

$$\mathrm{d}S_f = \frac{1}{K^2}\frac{Q}{A^2 R_h^{4/3}}\left(-2\frac{Q}{K}\mathrm{d}K - \frac{Q}{A}\left\{2 + \frac{4}{3}\left(1 - \frac{2R_h}{W_0}\right)\right\}\mathrm{d}A_0 + 2\mathrm{d}Q\right) - \mathrm{d}\phi(h) \tag{5}$$

with $\phi(h) = \frac{4}{3R_h^{7/3}}\frac{Q^2}{K^2A^2}\mathrm{d}f(h)$ a function depending on the observed geometry of a cross section above low flow and of the simulated flow (A, Q hence $h\,(A)$ given a channel geometry). We rewrite equation 5 as $\mathrm{d}S_f = \partial_K S_f \mathrm{d}K + \partial_{A_0} S_f \mathrm{d}A_0 + \partial_Q S_f \mathrm{d}Q - \mathrm{d}\phi(h)$ and under our modeling hypothesis we have $\partial_K S_f < 0$, $\partial_{A_0} S_f < 0$, $\partial_Q S_f > 0\ \forall x, t$, i.e. opposite effects of local values of friction K, low flow area A_0 and simulated local discharge Q values on S_f. Those terms are plotted on figure 9 along the Xingu River, on model grid, from hydraulic variables simulated (forward run) with calibrated parameters (cf. table 1). Note that $\mathrm{d}\phi(h)$ is not studied with this simple method.

Interestingly, $|\partial_K S_f|$ is about 100 times greater than $|\partial_{A_0} S_f|$ or $|\partial_Q S_f|$ at high flow and about 10 times greater at low flow. This is consistent with the singular value of friction that is found 1000 times greater than the one of reach averaged discharges by Garambois and Monnier [28] through a singular value decomposition of the normal equations of reach averaged Manning equations - applied to 70km of the Garonne River downstream of Toulouse (France). In other words, the friction term in the present modeling context must be more sensitive to a change in friction than unknown low-flow bathymetry or discharge.

Remark that for low-flow, S_f is more sensitive to discharge than unknown cross sectional area ($|\partial_Q S_f| > |\partial_{A_0} S_f|$) and conversely for high-flow. Moreover the spatial variability of the three sensitivities is more pronouced at low flow. Abrupt changes are found at locations corresponding to bottom slope or channel width changes. The influences of the bottom slope break at $x = 30$km is clearly visible at low-flow and the influence of the width contraction at $x = 17$km at high flow, which is fully consistent with the findings of Montazem et al. [46]. Further investigations on the sensitivity of the full Saint-Venant equations in space and time could be of interest to better taylor and constrain methods for tackling hydraulic inverse problems.

6. Conclusion

This paper investigates the challenging inference of the hydraulic triplet (discharge, bathymetry, friction) from real or synthetic altimetric WS observations only on an ungauged multichannel river.

The HiVDI inverse method presented in Larnier et al. [42] is adapted for reproducing a multichannel flow by introducing *a spatially distributed* friction law depending on modeled water depth h and by using multi-satellite

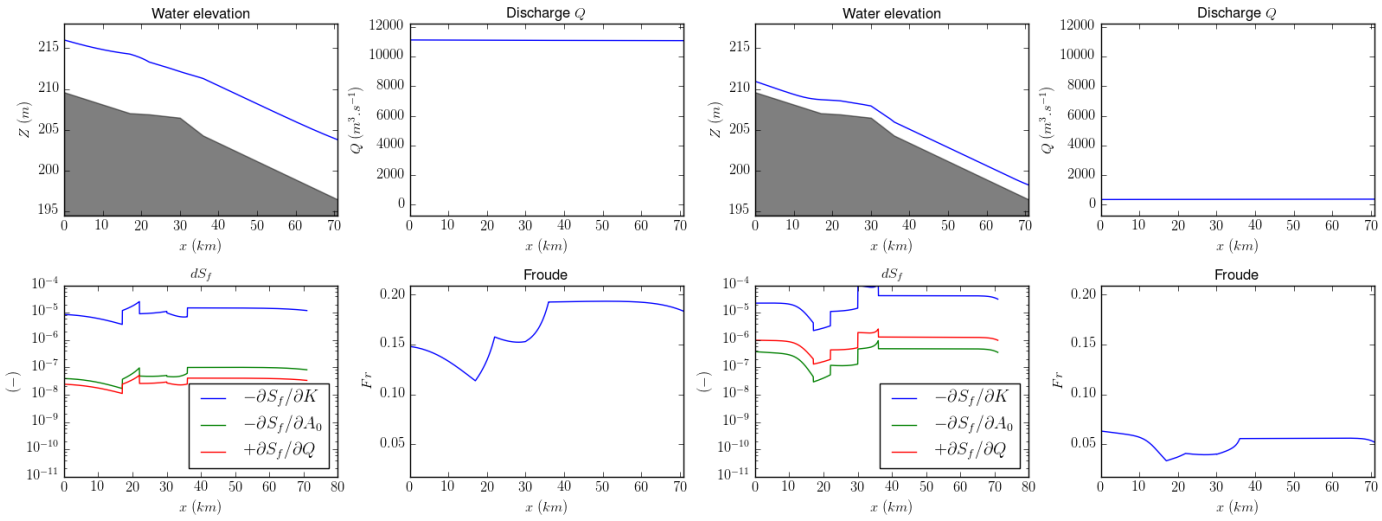

Figure 9: Evaluation of the partial derivatives of the friction source term S_f; forward run with the calibrated parameter set (cf. table 1) and true inflow discharge.

data.

The friction law coefficients are spatialized by reach to be coherent with the observation grid and with the (rather large) meaningful scale of these parameters in the 1D Manning-Strickler equation (see e.g. Guinot and Cappelaere [34]). This effective modeling approach enables a fairly accurate reproduction of the multichannel flows observed during 8 years by nadir altimetry (ENVISAT) on this $71km$ braided river.

The inference capabilities of hydraulic parameters patterns from real altimetric observations along a single ENVISAT track or from the future spatially dense SWOT observations are demonstrated. For the present observed multichannel river complexity, the inverse method enables to infer a fairly realistic upstream discharge hydrograph along with an effective river channel. The estimated bathymetry and friction patterns somehow result in local and effective stage-discharge relationships. In case of spatially sparse observations, the coherence between the sparse observation grid and the dense model grid is ensured using a piecewise linear bathymetry representation along with a friction power law with piecewise constant parameters. This constrain on the VDA process provided by the above defined effective bathymetry-friction representation by reach is highlighted with spatially sparse ENVISAT observations. Moreover the additional constrain provided by the forthcoming SWOT observations to infer a discharge hydrograph and densely distributed spatial controls is assessed on this effective multichannel river representation; the definition of friction by reaches enabling to consider more dense bathymetry controls.

SWOT observations would represent unprecedented measurements of hydraulic processes signatures from the local to the hydrographic network scales, including complex flow zones such as braided ones. On-going researches focus on the detection and use of various hydraulic signatures in WS as highlighted here for bottom slope (resp. channel width) breaks in low (resp. high) flows (see WS curvature analysis and SW model behavior in Montazem et al. [46]), on the estimation of reliable priors and inverse problems at the scale of larger river network portions including complex flow zones.

Author contributions and acknowledgments

The contributions of the respective authors are as follows. Pierre-André Garambois designed the research plan and performed the numerical investigations and analysis. Pierre-André Garambois, Pascal Finaud-Guyot, Kevin Larnier and Amanda Montazem contributed to the hydraulic understanding and sensitivity analysis. Jérôme Monnier is the principal designer of the inverse computational method and its analysis. Jonas Verley has started the present study during the beginning of his PhD. This study is warmly dedicated to him.

The computational software DassFlow1D and satellite data curation toolbox were adapted from their previous versions (Larnier et al. [42]) by Jonas Verley, Pierre-André Garambois and Kevin Larnier, this last generated the SWOT synthetic data using the large scale simulator and computational ressources of CNES ("Centre National d'Etudes Spatiales", French space agency); Amanda Montazem processed and analyzed the SWOT data. Stephane Calmant provided the multisatelite dataset and interesting discussions related to the concept of hydraulic visibility.

The authors K. Larnier (software engineer at CS corp.) and J. Verley (software engineer during 10 months next PhD student IMT-INSA-CLS 17-18) have been co-funded by CNES. The four other authors have been partly supported by CNES TOSCA research project 14-18. The authors are indebted to Adrien Paris and Joecilla Da Silva for sharing data and for fruitfull discussions.

7. Appendix: the computational inverse method

As already briefly summarized in Section 2.3, the computational inverse method is based on Variational Data Assimilation (VDA) applied to the Saint-Venant flow model (1). The computational inverse method is those presented in Brisset et al. [10], Larnier et al. [42] with an augmented composite control vector c, see (3): c contains a spatially distributed friction coefficient enabling to model complex flow zones (while it is an uniform friction law $K(h)$ in Larnier et al. [42]). This definition of $K(x,h)$ enables to consider more heterogeneous bathymetry controls.

It is important to point out that the imposed downstream boundary condition is an unknown of the inverse problem. It is constrained with the observed water elevations and infered river bottom slope using a locally uniform flow hypothesis (i.e. Manning equation, cf. section 2.1).

The cost function $j(c)$ is defined as:

$$j(c) = j_{obs}(c) + \gamma\, j_{reg}(c) \tag{6}$$

where $\gamma > 0$ is a weighting coefficient of the so-called "regularization term" $j_{reg}(c)$. The term $j_{obs}(c)$ measures the misfit between observed and modeled WS elevations such that:

$$j_{obs}(c) = \frac{1}{2}\,\|(Z(\mathrm{c}) - Z_{obs})\|^2_{\mathcal{O}} \tag{7}$$

The norm $\|\cdot\|_{\mathcal{O}} = \|\mathcal{O}^{1/2}\cdot\|_2$ is defined from an a-priori positive definite covariance matrix $\mathcal{O}$. Assuming uncorrelated observations $\mathcal{O} = diag(\sigma_Z)$ with σ_Z the a-priori observation error on Z_{obs} - $\sigma_Z = 15cm$ in this study.

The modeled WS elevations Z depend on c through the hydrodynamic model (1) and the inverse problem reads as

$$c^* = \text{argmin}_{\text{c}}\ \text{j}(c) \tag{8}$$

This optimal control problem is solved using a Quasi-Newton descent algorithm: the L-BFGS algorithm version presented in 31. The cost gradient $\nabla j(c)$ is computed by solving the adjoint model; the latter is obtained by automatic differentiation using Tapenade software [37]. Detailed know-hows on VDA may be found e.g. in the online courses Bouttier and Courtier [9], Monnier [44].

To be solved efficiently this optimization problem needs to be "regularized". Indeed the friction and the bathymetry may trigger indiscernible surface signatures therefore leading to an ill-posed inverse problem; we refer e.g. to Kaltenbacher et al. [40] for the theory of regularization of such inverse problems and to Larnier et al. [42] for a discussion focused on the present inverse flow problem.

Following Larnier et al. [42], the optimization problem (8) is regularized as follows. First the regularization term j_{reg} is added to the cost function, see (6). We simply set: $j_{reg}(c) = \frac{1}{2}\left\|b"(x)\right\|_2^2$. Therefore this term imposes (as weak constrains) the infered bathymetry profile $b(x)$ to be an elastic interpolating the values of b at the control points (i.e. a cubic spline).

A specificity of the present context is the large inconsistency between the large observation grid (altimetry points) and the finer finer model grid. Between the sparse observations points (equivalently the control points), the bathymetry profile $b(x)$ is reconstructed as a piecewise linear function. It is worth to point out that the resulting reconstruction is consistent with the physical analysis presented in Montazem et al. [47], Montazem et al. [46], Montazem [45]. (This study analyses the adequation between the SW model (1) behavior and the WS signature).

Next and following Lorenc et al. [43], Weaver and Courtier [57], Larnier et al. [42], the following change of control variable is made:

$$k = B^{-1/2}(\text{c} - \text{c}_{prior}) \tag{9}$$

where c is the original control vector, c_{prior} is a prior value of c and B is a covariance matrix. The choice of B is crucial in the VDA formulation; its expression is detailed below. After this change of variable the new optimization problem reads:

$$\min_k \text{J}(k) \text{ with } \text{J}(k) = j(c) \tag{10}$$

It is easy to show that this leads to the following new optimality condition: $B^{1/2}\nabla j(c) = 0$; somehow a

preconditioned optimality condition. For more details and explanations we refer to 35, 36 and Larnier et al. [42] in the present inversion context.

Assuming uncorrelated controls B is defined as a block-diagonal matrix:

$$B = \begin{pmatrix} B_Q & 0 & 0 & \\ 0 & B_b & 0 & \\ 0 & 0 & B_\alpha & \\ 0 & 0 & 0 & B_\beta \end{pmatrix} \tag{11}$$

Still following Larnier et al. [42], the matrices B_Q and B_b are set as the classical second order auto-regressive correlation matrices :

$$(B_Q)_{i,j} = (\sigma_Q)^2 \exp\left(-\frac{|t_j - t_i|}{\Delta t_Q}\right) \text{ and } (B_b)_{i,j} = (\sigma_b)^2 \exp\left(-\frac{|x_j - x_i|}{L_b}\right) \tag{12}$$

The VDA parameters Δt_Q and L_b represent prior hydraulic scales and act as correlation lengths. Given the frequency (few days) and spatial resolution of observations (200m long "pixels" for SWOT), the low Froude braided river flows of interest, adequate values for those parameters are: $\Delta t_Q = 24$ h and $L_b = 3km$ km We refer to Brisset et al. [10] for a thorough analysis of the discharge inference in terms of frequencies and wave lengths and Section 4.1 in the present river-observation context. In the present study, the friction parameters applied to deca-kilometric patches are assumed to be uncorrelated thus the matrices B_α and B_β are diagonal:

$$(B_\alpha)_{i,i} = (\sigma_\alpha)^2, (B_\beta)_{i,i} = (\sigma_\beta)^2 \tag{13}$$

The scalar values $\sigma_\square$ may be viewed as variances ; their values are given in the numerical results section.

8. References

[1] Allen, G. H., Pavelsky, T. M., 2018. Global extent of rivers and streams. Science.
URL http://science.sciencemag.org/content/early/2018/06/27/science.aat0636

[2] Alsdorf, D. E., Lettenmaier, D. P., 2003. Tracking fresh water from space. Science 301 (5639), 1491–1494.
URL http://www.sciencemag.org/content/301/5639/1491.short

[3] Andreadis, K. M., Clark, E. A., Lettenmaier, D. P., Alsdorf, D. E., 2007. Prospects for river discharge and depth estimation through assimilation of swath-altimetry into a raster-based hydrodynamics model. Geophysical Research Letters 34 (10).
URL https://agupubs.onlinelibrary.wiley.com/doi/abs/10.1029/2007GL029721

[4] Biancamaria, S., Durand, M., Andreadis, K., Bates, P., Boone, A., Mognard, N., Rodriguez, E., Alsdorf, D., Lettenmaier, D., Clark, E., 2011. Assimilation of virtual wide swath altimetry to improve arctic river modeling. Remote Sensing of Environment 115 (2), 373 – 381.
URL http://www.sciencedirect.com/science/article/pii/S0034425710002816

[5] Biancamaria, S., Lettenmaier, D. P., Pavelsky, T. M., Mar 2016. The swot mission and its capabilities for land hydrology. Surveys in Geophysics 37 (2), 307–337.
URL http://dx.doi.org/10.1007/s10712-015-9346-y

[6] Birkett, C. M., 1998. Contribution of the topex nasa radar altimeter to the global monitoring of large rivers and wetlands. Water Resources Research 34 (5), 1223–1239.
URL https://agupubs.onlinelibrary.wiley.com/doi/abs/10.1029/98WR00124

[7] Bjerklie, D. M., Birkett, C. M., Jones, J. W., Carabajal, C., Rover, J. A., Fulton, J. W., Garambois, P.-A., 2018. Satellite remote sensing estimation of river discharge: Application to the yukon river alaska. Journal of Hydrology 561, 1000 – 1018.
URL http://www.sciencedirect.com/science/article/pii/S0022169418302464

[8] Bjerklie, D. M., Dingman, S. L., Bolster, C. H., 2005. Comparison of constitutive flow resistance equations based on the manning and chezy equations applied to natural rivers. Water Resources Research 41 (11).
URL https://agupubs.onlinelibrary.wiley.com/doi/abs/10.1029/2004WR003776

[9] Bouttier, F., Courtier, P., 2002. Data assimilation concepts and methods march 1999. Meteorological training course lecture series. ECMWF, 59.

[10] Brisset, P., Monnier, J., Garambois, P.-A., Roux, H., 2018. On the assimilation of altimetric data in 1d saint–venant river flow models. Advances in water resources 119, 41–59.

[11] Cacuci, D., , Navon, I., , Ionescu-Bugor, M., 2013. Computational Methods for Data Evaluation and Assimilation. Taylor and Francis CRC Press: Boca Raton.

[12] Calmant, S., Cretaux, J.-F., Remy, F., 2016. 4 - principles of radar satellite altimetry for application on inland waters. In: Baghdadi, N., Zribi, M. (Eds.), Microwave Remote Sensing of Land Surface. Elsevier, pp. 175 – 218.
URL https://www.sciencedirect.com/science/article/pii/B9781785481598500049

[13] Calmant, S., Seyler, F., Cretaux, J., 2008. Monitoring continental surface waters by satellite altimetry. Surveys in Geophysics 29 (4-5), 247–269.
URL http://dx.doi.org/10.1007/s10712-008-9051-1

[14] Chow, V., 1959. Open-channel Hydraulics. Mc Graw-Hill, New-York, USA.

[15] Chow, V., 1964. Handbook of applied hydrology. McGraw-Hill Book Co., New-York, 1467 pages.

[16] Cunge, J. A., Holly, F., M., Verwey, A., 1980. Practical Aspects of Computational River Hydraulics. Pitam Publishing,.

[17] Da Silva, J. S., Seyler, F., Calmant, S., Rotunno Filho, O. C., Roux, E., AraÃÂºjo, A. A. M., Guyot, J. L., 2012. Water level dynamics of amazon wetlands at the watershed scale by satellite altimetry. International Journal of Remote Sensing 33 (11), 3323–3353.
URL http://dx.doi.org/10.1080/01431161.2010.531914

[18] de Paiva, R. C. D., Buarque, D. C., Collischonn, W., Bonnet, M., Frappart, F., Calmant, S., Mendes, C. A. B., 2013. Largeâscale hydrologic and hydrodynamic modeling of the amazon river basin. Water Resources Research 49 (3), 1226–1243.
URL https://agupubs.onlinelibrary.wiley.com/doi/abs/10.1002/wrcr.20067

[19] Durand, M., Andreadis, K. M., Alsdorf, D. E., Lettenmaier, D. P., Moller, D., Wilson, M., 2008. Estimation of bathymetric depth and slope from data assimilation of swath altimetry into a hydrodynamic model. Geophysical Research Letters 35 (20).
URL https://agupubs.onlinelibrary.wiley.com/doi/abs/10.1029/2008GL034150

[20] Durand, M., Gleason, C., Garambois, P.-A., Bjerklie, D., Smith, L., Roux, H., Rodriguez, E., Bates, P., Pavelsky, T., Monnier, J., et al., 2016. An intercomparison of remote sensing river discharge estimation algorithms from measurements of river height, width, and slope. Water Resources Research.

[21] Durand, M., Neal, J., Rodríguez, E., Andreadis, K. M., Smith, L. C., Yoon, Y., 2014. Estimating reach-averaged discharge for the river severn from measurements of river water surface elevation and slope. Journal of Hydrology 511, 92–104.

[22] et al., W. M. O., 2016. The global observing system for climate: Implementation needs.
URL library.wmo.int/doc$_num.php?explnum_id = 3417$

[23] Fekete, B., Vorosmarty, C., 2002. The current status of global river discharge monitoring and potential new technologies complementing traditional discharge measurements. IAHS - PUB.

[24] Ferguson, R., 2007. Flow resistance equations for gravel- and boulder-bed streams. Water Resources Research 43 (5).
URL https://agupubs.onlinelibrary.wiley.com/doi/abs/10.1029/2006WR005422

[25] Frappart, F., Calmant, S., Cauhope, M., Seyler, F., Cazenave, A., 2006. Preliminary results of envisat ra-2-derived water levels validation over the amazon basin. Remote Sensing of Environment 100 (2), 252 – 264.
URL http://www.sciencedirect.com/science/article/pii/S0034425705003585

[26] Frasson, R. P. d. M., Wei, R., Durand, M., Minear, J. T., Domeneghetti, A., Schumann, G., Williams, B. A., Rodriguez, E., Picamilh, C., Lion, C., Pavelsky, T., Garambois, P.-A., 2017. Automated river reach definition strategies: Applications for the surface water and ocean topography mission. Water Resources Research 53 (10), 8164–8186.
URL http://dx.doi.org/10.1002/2017WR020887

[27] Garambois, P.-A., Calmant, S., Roux, H., Paris, A., Monnier, J., Finaud-Guyot, P., Samine Montazem, A., Santos-da Silva, J., 2017. Hydraulic visibility: Using satellite altimetry to parameterize a hydraulic model of an ungauged reach of a braided river. Hydrological Processes 31 (4), 756–767, hyp.11033.
URL http://dx.doi.org/10.1002/hyp.11033

[28] Garambois, P.-A., Monnier, J., 2015. Inference of effective river properties from remotely sensed observations of water surface. Advances in Water Resources 79, 103–120.

[29] Gejadze, I., Malaterre, P.-O., 2017. Discharge estimation under uncertainty using variational methods with application to the full saint-venant hydraulic network model. International Journal for Numerical Methods in Fluids 83 (5), 405–430, fld.4273.
URL http://dx.doi.org/10.1002/fld.4273

[30] Gessese, A. F., Sellier, M., Van Houten, E., Smart, G., 2011. Reconstruction of river bed topography from free surface data using a direct numerical approach in one-dimensional shallow water flow. Inverse Problems 27 (2), 025001.
URL http://stacks.iop.org/0266-5611/27/i=2/a=025001

[31] Gilbert, J. C., Lemaréchal, C., 1989. Some numerical experiments with variable-storage quasi-newton algorithms. Mathematical programming 45 (1-3), 407–435.

[32] Gleason, C. J., Smith, L. C., 2014. Toward global mapping of river discharge using satellite images and at-many-stations hydraulic geometry. Proceedings of the National Academy of Sciences 111 (13), 4788–4791.
URL http://www.pnas.org/content/111/13/4788

[33] Guinot, V., 1993. Wave Propagation in Fluids: Models and Numerical Techniques. Vol. 16.

[34] Guinot, V., Cappelaere, B., 2009. Sensitivity equations for the one-dimensional shallow water equations: Practical application to model calibration. Journal of Hydrologic Engineering 14 (8), 858–861.
URL

[35] Haben, S. A., Lawless, A. S., Nichols, N. K., 2011. Conditioning and preconditioning of the variational data assimilation problem. Computers & Fluids 46 (1), 252–256.

[36] Haben, S. A., Lawless, A. S., Nichols, N. K., 2011. Conditioning of incremental variational data assimilation, with application to the met office system. Tellus A 63 (4), 782–792.

[37] Hascoët, L., Pascual, V., 2013. The Tapenade Automatic Differentiation tool: Principles, Model, and Specification. ACM Transactions On Mathematical Software 39 (3).
URL http://dx.doi.org/10.1145/2450153.2450158

[38] Honnorat, M., Lai, X., le Dimet, F.-X., Monnier, J., 2006. Variational data assimilation for 2D fluvial hydraulics simulation. CMWR XVI-Computational Methods for Water Ressources. Copenhagen, june 2006.

[39] Hostache, R., Lai, X., Monnier, J., Puech, C., 2010. Assimilation of spatially distributed water levels into a shallow-water flood model. Part II: Use of a remote sensing image of Mosel River. Journal of Hydrology 390, 257–268, 3-4.
URL http://www.sciencedirect.com/science/article/pii/S0022169410004166

[40] Kaltenbacher, B., Neubauer, A., Scherzer, O., 2008. Iterative regularization methods for nonlinear ill-posed problems. Vol. 6. Walter de Gruyter.

[41] Lai, X., Monnier, J., 2009. Assimilation of spatially distributed water levels into a shallow-water flood model. Part I: mathematical method and test case. Journal of Hydrology 377, 1–11, 1-2.
URL http://www.sciencedirect.com/science/article/pii/S0022169409004508

[42] Larnier, K., Monnier, J., Garambois, P.-A., Verley, J., 2019. River discharge and bathymetry estimations from swot altimetry measurements. - -, –.

[43] Lorenc, A., Ballard, S., Bell, R., Ingleby, N., Andrews, P., Barker, D., Bray, J., Clayton, A., Dalby, T., Li, D., et al., 2000. The met. office global three-dimensional variational data assimilation scheme. Quarterly Journal of the Royal Meteorological Society 126 (570), 2991–3012.

[44] Monnier, J., 2014. Variational data assimilation: from optimal control to large scale data assimilation. Open Online Course, INSA Toulouse.

[45] Montazem, A., 2018. Representation et segmentation hydraulique effective de rivieres pour le calcul de debit par altimetrie swot Ã l'echelle globale. ThÃšse de doctorat, Universite de Toulouse III Paul Sabatier, Toulouse, France.

[46] Montazem, A., Garambois, P.-A., Finaud-Guyot, P., Calmant, S., Monnier, J., Moreira, D., 2018. Physical basis for river segmentation from water surface observables. revised -, –.

[47] Montazem, A. S., Garambois, P.-A., Calmant, S., Medeiros Moreira, D., Monnier, J., Biancamaria, S., 2017. Physical basis for river segmentation. In: AGU fall metting.

[48] Oubanas, H., Gejadze, I., Malaterre, P.-O., Mercier, F., 2018. River discharge estimation from synthetic swot-type observations using var- iational data assimilation and the full saint-venant hydraulic model. Journal of Hydrology, Accepted, to appear.

[49] Paris, A., Dias de Paiva, R., Santos da Silva, J., Medeiros Moreira, D., Calmant, S., Garambois, P.-A., Collischonn, W., Bonnet, M.-P., Seyler, F., 2016. Stage-discharge rating curves based on satellite altimetry and modeled discharge in the amazon basin. Water Resources Research 52 (5), 3787–3814.
URL https://agupubs.onlinelibrary.wiley.com/doi/abs/10.1002/2014WR016618

[50] Rodriguez, E., 2012. SWOT Science requirements document. JPL document, JPL.

[51] Roux, H., Dartus, D., 2006. Use of parameter optimization to estimate a flood wave: Potential applications to remote sensing of rivers. J. of Hydrology 328, 258–266.

[52] Schneider, R., Godiksen, P. N., Villadsen, H., Madsen, H., Bauer-Gottwein, P., 2017. Application of cryosat-2 altimetry data for river analysis and modelling. Hydrology and Earth System Sciences 21 (2), 751–764.
URL https://www.hydrol-earth-syst-sci.net/21/751/2017/

[53] Schubert, J. E., Monsen, W. W., Sanders, B. F., 2015. Metric-resolution 2d river modeling at the macroscale: Computational methods and applications in a braided river. Frontiers in Earth Science 3, 74.
URL https://www.frontiersin.org/article/10.3389/feart.2015.00074

[54] Schumann, G. J.-P., Domeneghetti, A., 2016. Exploiting the proliferation of current and future satellite observations of rivers. Hydrological Processes 30 (16), 2891–2896.
URL https://onlinelibrary.wiley.com/doi/abs/10.1002/hyp.10825

[55] Tuozzolo, S., Lind, G., Overstreet, B., Mangano, J., Fonstad, M., Hagemann, M., Frasson, R. P. M., Larnier, K., Garambois, P.-A., Monnier, J., Durand, M., 2019. Estimating river discharge with swath altimetry: A proof of concept using airswot observations. Geophysical Research Letters 0 (ja).
URL https://agupubs.onlinelibrary.wiley.com/doi/abs/10.1029/2018GL080771

[56] Vorosmarty, C. J., Willmott, C. J., Choudhury, B. J., Schloss, A. L., Stearns, T. K., Robeson, S. M., Dorman, T. J., 1996. Analyzing the discharge regime of a large tropical river through remote sensing, ground-based climatic data, and modeling. Water Resour. Res. 32, 3137–3150, 10.
URL http://dx.doi.org/10.1029/96WR01333

[57] Weaver, A., Courtier, P., 2001. Correlation modelling on the sphere using a generalized diffusion equation. Quarterly Journal of the Royal Meteorological Society 127 (575), 1815–1846.

664 [58] Yoon, Y., Durand, M., Merry, C., Clark, E., Andreadis, K., D.E., A., 2012. Estimating river bathymetry from
665 data assimilation of synthetic swot measurements. Journal of Hydrology 464 - 465 (0), 363 – 375.
666 URL http://www.sciencedirect.com/science/article/pii/S0022169412006294

667 [59] Yoon, Y., Garambois, P.-A., Paiva, R., Durand, M., Roux, H., Beighley, E., 2016. Improved error estimates of
668 a discharge algorithm for remotely sensed river measurements: Test cases on Sacramento and Garonne Rivers.
669 Water Resources Research 52 (1), 278–294.